Raman study of individually dispersed single-walled carbon nanotubes under pressure

Sergei Lebedkin,[1,*] Katharina Arnold,[1,2] Oliver Kiowski,[1,2] Frank Hennrich,[1] and Manfred M. Kappes[1,2]
[1]*Forschungszentrum Karlsruhe, Institut für Nanotechnologie, D-76021 Karlsruhe, Germany*
[2]*Institut für Physikalische Chemie, Universität Karlsruhe, D-76128 Karlsruhe, Germany*
(Received 24 November 2005; revised manuscript received 18 January 2006; published 9 March 2006)

We report the resonant Raman spectra of individualized (=*debundled*) single-walled carbon nanotubes (SWNTs) having diameters $d \sim 0.8-1.3$ nm subject to compression up to 10.5 GPa. Both SWNTs in water-surfactant dispersions as well as SWNTs deposited onto glass microfibers and compressed with methanol-ethanol were studied. In the low pressure regime (<1 GPa), linear and reversible up-shifts of the Raman bands associated with the radial breathing vibrational mode (RBM) and tangential G mode were observed. The pressure derivative of the RBM frequency increases with increasing d and, unexpectedly, is larger for metallic than for semiconducting tubes. Above 1–2 GPa, RBM bands of additional SWNT species appear. This is due to pressure-induced shifts into resonance and broadening of the corresponding optical transitions. The latter could be quantified by photoluminescence (PL) measurements of the corresponding semiconducting tubes that are also reported here. Disappearance of the RBM and G bands contributed by nanotubes with $d \sim 0.8-0.9$ and $\sim 1.2-1.3$ nm at ~ 10 and ~ 4 GPa, respectively, is tentatively assigned to extensive radial deformation of the nanotubes, in accordance with theoretical predictions. After the application of several GPa pressure, a significant loss of Raman signals and a relative increase of the defect-induced D band are found, in particular for metallic SWNTs. We attribute these and other irreversible effects in the Raman spectra to defects generated in nanotubes under compression (most likely via chemical processes). Comparable structural deterioration of semiconducting nanotubes is evidenced by strong irreversible changes in their PL spectra.

DOI: 10.1103/PhysRevB.73.094109 PACS number(s): 61.46.−w, 62.50.+p

I. INTRODUCTION

The extraordinary mechanical properties of SWNTs, including their high Young's modulus, excellent axial strength, and flexibility, are of significant interest both for basic research and for potential applications.[1] High pressure studies represent a potentially useful approach to investigate the mechanical resilience of carbon nanotubes under extreme stress conditions and, more specifically, the influence of pressure-induced structural deformation on the electronic/optical properties of nanotubes. A particularly important issue is radial deformation and collapse of SWNTs subject to hydrostatic compression, i.e., distortion of a tube circular cross section to an oval (flattened) shape,[2] which is generally expected for hollow tubular structures at some critical external pressure. Ideally, SWNTs may reversibly sustain such a large deformation.[3] However, mechanical, electronic, as well as chemical properties are expected to be dramatically affected by collapse, conceivably leading to irreversibility via reactions with the environment.

The radial deformation and collapse of nanotubes under hydrostatic pressure has been considered in numerous theoretical[4–17] and experimental[15–27] studies. Onset of a circular-to-oval structural transition at critical pressure P_C was consistently predicted by classical molecular dynamics (MD) calculations in model SWNT bundles[13,17] as well as in individual nanotubes.[10,12,14] A very recent MD study of Tangney *et al.* predicts complex scenarios of nanotube deformation, ranging from continuous deformation into a flattened shape for small diameter tubes ($d \sim 0.8$ nm) to abrupt collapse and hysteresis effects (metastable states) upon the pressure decrease for large diameter tubes ($d \sim 1.5$ nm).[14] An important result of the MD calculations is a weak dependence of P_C on nanotube helicity, but a strong dependence on nanotube diameter, approximated for individual nanotubes as $P_C \sim 1/d^{\alpha}$, $\alpha \sim 2.9-3$.[10,12,14] Specifically, for SWNTs produced by the HiPco method with $d \sim 0.8-1.3$ nm, the corresponding ranges of P_C are $\sim 7-2$ GPa and $\sim 5-1$ GPa according to Capaz *et al.*[10] and Sun *et al.*,[12] respectively. The last values may be underestimated by a factor of 2, as was indicated by a reference *ab initio* MD calculation.[12] Similar values of P_C vs d were also predicted by MD for bundled nanotubes[13,15,17] and by a simple structural mechanics model for individual nanotubes.[11] Note that the broad intervals of P_C expected for the available SWNT materials (=wide diameter distributions) makes an experimental determination of the structural transition(s) nontrivial, especially when the experiment probes integral parameters like bundle size and packing. As we discuss in detail later, optical spectroscopy has an advantage in this respect, since groups of a few nanotube species or even specific types of SWNT [defined by two structural indices (n,m)] can be selectively excited and monitored.

Sophisticated *ab initio* calculations[7–9] performed for model crystalline SWNT bundles agree satisfactorily with the MD studies as far as the characteristic transition pressure is concerned. Reich *et al.* predicted the circular-to-oval structural transition for SWNTs with d ~ 0.8 nm at 9–15 GPa, depending on nanotube helicity.[9] A similar transition in a bundle of (10,10) tubes ($d=1.36$ nm) was established by Chan *et al.* at $P_C \sim 2.7$ GPa.[7] Sluiter *et al.* found a symmetry-dependent hexagonal deformation of nanotubes conforming to their triangular lattice packing in bundles. However, according to Chan *et al.* and Reich *et al.*, this state

is metastable and transforms into an oval shape. Under very high pressure, collapsed SWNTs in bundles may form covalent intertube links.[8,9]

Importantly, according to *ab initio* calculations of Okada *et al.*[4] for bundles and Gülseren *et al.*[6] for individual SWNTs, the electronic structure of nanotubes is highly sensitive to radial distortion. Even a moderate oval deformation can transform a semiconducting tube into a metallic one.[6] This would imply equally dramatic changes in the optical properties of nanotubes. For example, in a Raman experiment, a strong resonant enhancement present at atmospheric pressure would most likely break down for nanotubes deformed at elevated pressures and Raman signals would drop correspondingly.

High pressure experiments on SWNTs have been done by using x-ray[20,21] and neutron[22] diffraction, optical absorption[18] and resonant Raman spectroscopy[15–17,23–26] in combination with diamond anvil cell (DAC) techniques. Different types of SWNT samples have been studied, including as-prepared, nearly defect-free SWNTs as well as defect-rich SWNTs generated by oxidative purification (to remove metal catalyst and amorphous carbon particles). All of these samples were composed of *nanotube bundles* of different size and morphology. Taking into account the variations in materials type and sample history, it is not surprising that a wide spread of experimental results has been obtained. Thus, Tang *et al.* reported the decay of a bundle x-ray diffraction peak for as-prepared SWNTs at $\sim$1.5 GPa and attributed this to the hexagonal deformation of nanotubes in compressed bundles,[20] whereas Sharma *et al.* have observed this peak up to 10 GPa for chemically processed SWNTs.[21] Several Raman studies of as-prepared SWNTs with $d \sim 1-1.4$ nm reported a disappearance of the RBM band and a change in the pressure derivative of the *G* band frequency at 1.5–2 GPa, which was assigned to the hexagonal[15,16] or oval[17] cross-section deformation. On the other hand, the RBM bands of purified SWNTs with similar diameters were observed by Teredesai *et al.*[19] and Venkateswaran *et al.*[23] up to 4 and 7 GPa, respectively. Despite the persistent Raman signals to higher pressures, the latter authors discussed the possibility of a structural transition at $\sim$2 GPa in order to explain a drop of the RBM intensity observed there. An anomalous shift of the *G* band over the 10–16 GPa range has been assigned to the hexagonal distortion of SWNTs in Ref. 19. More recent work on bundled SWNTs has revised the previous estimates in favor of much higher values of collapse pressures. Amer *et al.* have demonstrated a dependence of the anomalous *G* band shift on pressure transmitting medium and have ruled out significant deformation of as-prepared SWNTs ($d \sim 1-1.4$ nm) below 10 GPa.[25] No sign of collapse, at least up to $\sim$13 GPa, has been observed by Monteverde and Núnez-Regueiro, who measured electrical transport through networks of as-grown SWNT bundles with $d \sim 1-1.5$ nm under hydrostatic compression.[27] Merlen *et al.* observed the RBM and *G* bands and their continual changes in purified SWNTs up to pressures as great as 10 and 40 GPa, respectively.[26] In this case, however, the nanotubes were "opened" by a harsh oxidative treatment so that argon (pressure transmitting medium) could freely fill their inner channels.[26] Furthermore, such oxidized nanotubes are likely covalently linked within bundles. Apparently, their mechanical and electronic properties deviate siginificantly from those of SWNT bundles before treatment. With regard to pressurization experiments, typical as-prepared SWNTs are generally thought to be "closed" and essentially empty. To our knowledge, no evidence has been put forward that such SWNTs can be filled with a (molecular) pressure transmitting medium like methanol-ethanol on the time scale of the high pressure/room temperature experiments.

Compared to the samples of bundled nanotubes studied so far, ensembles of *individualized* (debundled), as-prepared SWNTs are better-defined objects for high pressure experiments. Different individual nanotubes in such samples are expected to be similarly compressed in contrast to compression conditions across typical SWNT bundles. These are each composed of hundreds of nanotubes with various diameters that are likely nonuniformly distributed. Consequently, the interpretation of bundle measurements is subject to many assumptions. (In fact, nonuniform compression may be an additional reason for the conflicting results obtained for SWNT bundles.) Recently, an efficient method for ultrasonic exfoliation of SWNT bundles in water-surfactant dispersions and the separation of metallic and amorphous carbon impurities by centrifugation has been developed.[28] The majority of nanotubes ($>$50% according to our Raman data[29] and the AFM analysis of SWNTs deposited by spin-coating onto silicon[30]) in such dispersions are isolated as "individuals" in surfactant micelles and correspondingly manifest dominant and characteristic features in optical absorption and Raman spectra compared to contributions from SWNT bundles. Furthermore, individualized semiconducting SWNTs demonstrate near-infrared bandgap photoluminescence (PL).[31] Because of the relatively sharp optical transitions in dispersed SWNTs [broadened and shifted by intertube interactions in bundles (which also quench PL)],[32] specific (n,m) nanotubes can be addressed in the Raman and PL spectra by choosing the appropriate excitation wavelength.

In this paper we report the first Raman investigation of pressure effects on individually dispersed (debundled) HiPco nanotubes compressed up to $\sim$10 GPa. Laser wavelengths of 514, 633, and 785 nm were used to excite different metallic and semiconducting nanotubes and to determine (n,m) dependence of the RBM frequency shifts under hydrostatic compression. Because of local shear stresses, i.e., nonhydrostatic conditions, occurring in solidified aqueous suspensions under high pressure,[33] we also measured Raman spectra of individually dispersed nanotubes deposited onto glass microfibers from the same suspensions (without rebundling) and then pressurized using a methanol-ethanol mixture as the compression medium.

We will present and discuss results on the evolution of the RBM and *G* bands of dispersed/deposited SWNTs under high pressure—taking into account pressure-induced shifts and broadenings of optical transitions as estimated from PL data, which were also acquired in this study. In particular, we consider the implications of the Raman spectra for the possible structural deformation (collapse) as well as for other types of irreversible damage of SWNTs after the application of high pressure.

II. EXPERIMENTS

The "as-prepared" SWNT material used in this study was produced at Rice University by the high pressure catalytic decomposition of carbon monoxide (HiPco process). The preparation of water-surfactant dispersions of individualized nanotubes (estimated concentration ~10 μg/ml) by powerful sonication and ultracentrifugation has been described elsewhere.[29] The average SWNT length in dispersion was found to be ~200–300 nm by an AFM analysis of spin-coated silicon substrates. D_2O was frequently used instead of H_2O because of its broader transparency window in the near-infrared spectral range and the possibility to measure both Raman and near-infrared PL spectra for the same dispersion. The surfactants (typical concentration 0.5–1 wt.%) included sodium dodecylbenzene sulfonate (SDBS) and, primarily, sodium cholate, which yields particularly stable dispersions of SWNTs. Some experiments were performed with dispersions containing sodium dodecyl sulfate (SDS). Deposition of nanotubes onto glass microfibers (Whatman GF/A filter composed of a loose network of ~2 μm diameter approximately cylindrical glass fibers) was done by coating the latter with a diluted sodium cholate dispersion and subsequent vacuum drying. The surfactant was not washed out. Therefore nanotubes are likely embedded in a ~50 nm thick layer of the surfactant on glass microfibers. Raman and PL spectra of such deposited nanotubes were found to be similar to those of dispersions, indicating that the majority of deposited nanotubes were still in the isolated (debundled) form. This is in parallel to the conclusion derived in our recent work that normal spin coating of SWNT dispersions onto a silicon substrate does not lead to the pronounced rebundling of nanotubes.[29] Note also that a significant bundle content can be followed by characteristic signatures in the RBM Raman spectra.[29,32]

High pressure experiments were performed using two conventional screw-driven DACs (Diacell) designed for pressure ranges up to ~3 and ~20 GPa, respectively. The 0.25 mm thick gaskets made of stainless steel or Waspaloy were used. The tedious standard procedure of gasket preindentation was generally not applied, as mostly modest pressures were probed—in particular, in experiments using the low pressure DAC. Instead, a ready-to-use, laser-machined gasket having 0.5 or 0.2 mm central sample hole was positioned onto the lower diamond anvil with the aid of a miniature X-Y-Z stage, filled with the dispersion and sealed with the top anvil. This simple procedure required only a few minutes in order to assemble the DAC for a measurement. In the case of nanotubes on glass microfibers, a small piece of this material was placed into a gasket and then covered with an excess volume of methanol-ethanol (4:1 v/v) applied as the pressure transmitting medium. Ruby microcrystals were added for pressure calibration (via resolution of the shift in ruby R-line emission as excited at 633 nm). A typical compression-decompression experiment was performed within ~30 min.

Raman spectra were measured with a Witec CMA200 Raman microscope at laser excitation wavelengths of 514 and 633 nm. Samples in the low pressure DAC were also measured with a Kaiser Optical Systems HoloLab Raman spectrometer at $\lambda_{ex}=785$ nm. The spectral resolution and typical excitation intensity for both instruments were ~2 cm^{-1} and ~10 KW/cm^2, respectively. Photoluminescence spectra were obtained with a home-built near-infrared laser luminescence microscope. In this apparatus, a CW Ti-Sapphire laser (Spectra Physics) automatically scanned an excitation range of 708–860 nm in 1–2 nm steps at a controlled output power. At each excitation wavelength a PL spectrum was acquired using a liquid nitrogen cooled InGaAs photodiode array (~800–1600 nm) attached to a near-infrared spectrograph (Roper Scientific). The PL spectra measured were then combined into PL maps like that shown later in Fig. 10. All preparations and measurements were performed at room temperature.

III. RESULTS AND DISCUSSION

A. (n,m) assignment of RBM Raman spectra

The sharp optical transitions (FWHM ~40–60 meV in the visible spectral range)[32] of room temperature ensembles of individually dispersed SWNTs allow the selective excitation of only a few (n,m) species at a time, although the materials themselves contain tens of different types of SWNTs. Different (n,m) nanotubes excited at the same visible wavelength typically manifest distinct RBM frequencies, ω_{RBM}, which are approximately inversely proportional to tube diameter, d. Therefore, the (n,m)-dependent response of nanotubes to hydrostatic compression can be analyzed from the evolution of the RBM Raman spectra.

Figure 1 shows interband optical transition energies, E_{ii}, of nanotubes dispersed in water-SDS solutions as a function of ω_{RBM} (at ambient pressure). The ω_{RBM} range in Fig. 1 is characteristic for HiPco material and corresponds to tube diameters from ~0.7 to ~1.4 nm, whereas the energy range in Fig. 1 covers the first (E_{11}^M) and second (E_{22}^S) optical transitions of metallic and semiconducting nanotubes, respectively. These data are compiled from assignments of (E_{11}^S, E_{22}^S) vs (n,m) derived from photoluminescence spectra by Bachilo *et al.*[31] and of (E_{ii}, ω_{RBM}) vs (n,m) from resonant Raman spectra by Strano *et al.*,[34] Telg *et al.*,[35] and Fantini *et al.*[36] In addition, several higher energy E_{33}^S transtions (triangles) of large diameter semiconducting tubes show up in the plotted energy range. These data points derive from calculations by Barone *et al.*[37] Note, however, that the corresponding nanotubes are only minor species in HiPco material. For consistency, we computed RBM frequencies for all nanotubes shown in Fig. 1 from the fitting relations of Fantini *et al.*: ω_{RBM} $(cm^{-1})=A/d(nm)+B$, with coefficients $A=218$ cm^{-1}, $B=17$ cm^{-1} for metallic and $A=223$ cm^{-1}, $B=10$ cm^{-1} for semiconducting tubes, respectively.[36] A carbon-carbon bond length of 0.142 nm was used to calculate tube diameters.

Strictly speaking, the assignment of (E_{ii}, ω_{RBM}) vs (n,m) compiled in Fig. 1 is only valid for nanotubes dispersed with the surfactant SDS. For reasons discussed in Sec. III C, we excluded SDS dispersions from high pressure Raman experiments in favor of dispersions with sodium cholate or SDBS. When comparing individualized nanotube suspensions using

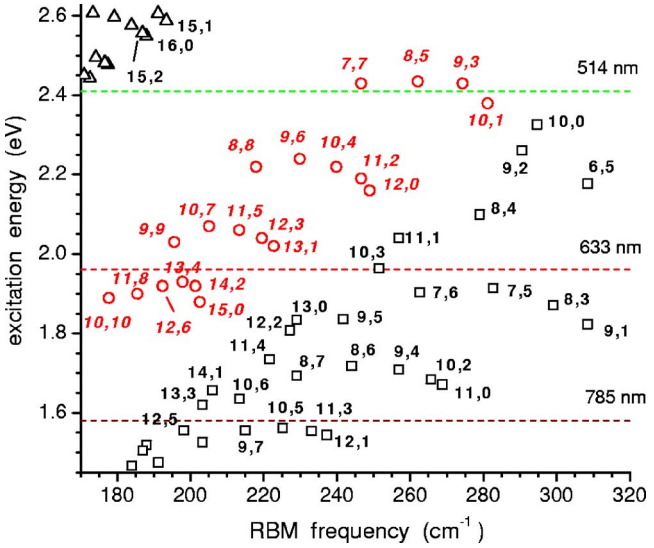

FIG. 1. (Color online) Optical interband transition (resonant Raman excitation) energies, E_{ii}, versus RBM frequencies, ω_{RBM}, for individualized (n,m) nanotubes dispersed in water—SDS. The E_{ii} and ω_{RBM} values as well as their (n,m) assignment are compiled from the photoluminescence study of Bachilo *et al.* (Ref. 31) and the Raman data of Telg *et al.* (Ref. 35) and Fantini *et al.* (Ref. 36). The plotted energy range covers the first (E_{11}^{M}) and second (E_{22}^{S}) transitions of metallic (circles and italic n,m indices) and semiconducting (squares) HiPco nanotubes, respectively. Triangles refer to the third interband transition energies (E_{33}^{S}) of semiconducting tubes, as calculated by Barone *et al.* (Ref. 37). The horizontal lines denote the laser excitation energies applied in this work.

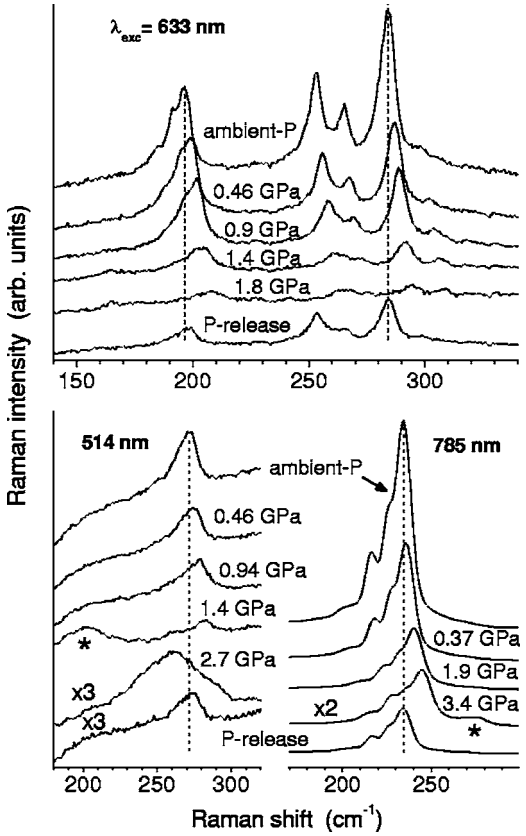

FIG. 2. The pressure dependence of Raman spectra in the RBM frequency range for HiPco nanotubes dispersed in water - 1 wt.% sodium cholate and excited at 633, 785, and 514 nm. The pressure was increased in steps of ~0.2 GPa up to the largest indicated value and then decreased. Each RBM pattern is contributed by several (n,m) nanotubes having optical transitions in resonance with the laser excitation line (Fig. 1). The asterisks indicate new resonant RBM features that appear due to pressure-induced shifts of optical transitions of corresponding nanotubes (see Sec. III C for details).

the three surfactants, we observed relatively small and nearly uniform, i.e., (n,m)-independent, shifts of the E_{11}^{S} and E_{22}^{S} energies (<20 meV) in the PL spectra, as well as only a minor variation of ω_{RBM} (<1%) in the Raman spectra. Consequently, at least for those regions of relatively low "density" of HiPco nanotubes per (E_{ii}, ω_{RBM}) spectral area, the assignment of Fig. 1 remains unequivocal and can be readily applied to SDBS and cholate suspensions also.

Figure 1 then allows the determination of which (n,m) nanotubes were probed in our experiments. Three groups of HiPco nanotubes with distinct electronic properties—a group of metallic tubes, a mixed group of metallic and semiconducting tubes, and a group of only semiconducting tubes—were probed by excitation at 514, 633, and 785 nm, respectively. Depending on their concentrations in dispersion, Raman cross sections, and resonance matching, not all nanotubes having optical transitions close to the excitation lines in Fig. 1 contribute equally to the Raman spectra. Strong (n,m) components were identified by Lorentzian peak fitting of the RBM Raman spectra at ambient pressure (Fig. 2) and by comparing with the assignment in Fig. 1. These nanotubes are listed in Table I. Figure 3(a) obtained for a cholate dispersion illustrates the fitting procedure for the RBM pattern excited at 633 nm. Two well-separated band structures with $\omega_{RBM} \sim 180-200$ and $\sim 250-300$ cm^{-1} correspond to three metallic and four semiconducting tubes within diameter ranges of ~1.2–1.3 and ~0.8–0.9 nm, respectively.

The same RBM bands were found in the spectra of dispersions containing SDBS and SDS. The RBM spectra at ambient pressure in Fig. 2 and, consequently, their (n,m) assignment agree well with published data,[35,36] indicating a reproducible composition of the dispersions of HiPco nanotubes. Note that the Raman spectra [and consequently an (n,m) assignment of contributing nanotubes] can be affected by shifts and broadening of optical transitions of SWNTs under pressure. These effects are discussed in Secs. III C and III G.

B. Shifts of RBM frequencies: Low pressure regime

Figure 2 presents the evolution of the RBM spectral region for applied pressures up to ~2–3 GPa for HiPco nanotubes in a water-sodium cholate dispersion—as obtained at different laser excitation wavelengths. Continuous frequency upshifts and a loss of intensity with increasing pressure are observed for the RBM bands assigned to different (n,m) nanotubes. These changes are essentially completely reversible after weak compression to below ~1 GPa, but become irreversible in part at higher pressures. For example, Fig. 2 shows that after the application of ~2–3 GPa pressure and

TABLE I. Pressure derivative of the RBM frequency, ω_{RBM}, versus the nanotube helicity index (n,m). Data are for HiPco nanotubes dispersed in water-sodium cholate under low pressure conditions ($\leqslant$1 GPa). Three groups of metallic and semiconducting (n,m) nanotubes were probed at laser excitation wavelengths of 514, 633, and 785 nm (from top to bottom). Italic (n,m) indices denote metallic nanotubes.

n,m	ω_{RBM},[a] cm^{-1}	Pressure derivative, cm^{-1}/GPa	Tube diameter,[b] nm
8,5	266	7.4±0.5	0.89
9,3	273	7.6±0.5	0.85
11,8	184	7.7±0.8	1.29
12,6	191	8.2±1.0	1.24
13,4 (14,2)[c]	197	7.4±0.8	1.20 (1.18)
10, 3	253	5.9±0.3	0.92
7, 6	265	5.2±0.5	0.88
7, 5	284	5.6±0.3	0.82
8, 3	299	5.2±0.4	0.77
9, 7	215	6.4±0.3	1.09
10, 5	225	6.2±0.4	1.04
11, 3	233	5.9±0.3	1.00
12, 1	237	6.0±0.3	0.98

[a]Accuracy ±1 cm^{-1}.
[b]Calculated using carbon-carbon bond length of 0.142 nm.
[c]RBM band can be assigned to both (n,m) species.

subsequent pressure release the RBM bands of semiconducting tubes (spectra at λ_{ex}=785 nm and a group of bands within $\omega_{RBM}\sim$250–300 cm^{-1} at λ_{ex}=633 nm) exhibit a significant decrease of intensity. The bands assigned to metallic nanotubes (overlapped bands at λ_{ex}=514 nm and a group of bands within $\omega_{RBM}\sim$180–200 cm^{-1} at λ_{ex}=633 nm) exhibit, not only a loss of intensity, but also a small frequency upshift after the release of pressure. Similar results were obtained for SWNTs in water-SDBS dispersions and for SWNTs deposited onto glass microfibers and compressed with methanol–ethanol. The irreversible changes in the Raman and PL spectra, as a result of increasing compression, are attributed to structural deterioration of nanotubes and are discussed in Secs. III E–III G. Note that these changes were observed for aqueoues dispersions compressed above the solidification pressure (~1 GPa at room temperature). The diffusion and rebundling of nanotubes are expected to be strongly hindered in solidified dispersions. Therefore we do not consider a possible increase in the bundle content due to compression as the major reason for irreversible effects in the Raman and PL spectra.

For pressures less than 1 GPa, the shifts of RBM frequencies were found to be linearly pressure dependent (within experimental error) as well as (n,m) dependent. This is illustrated in Fig. 3(b) for the RBM region as excited at 633 nm. A plot of the pressure derivative $d\omega_{RBM}/dP$ as a function of the tube diameter reveals an approximately linear increase of $d\omega_{RBM}/dP$ with increasing diameter for semiconducting tubes (Fig. 4, empty squares). The dependence for metallic

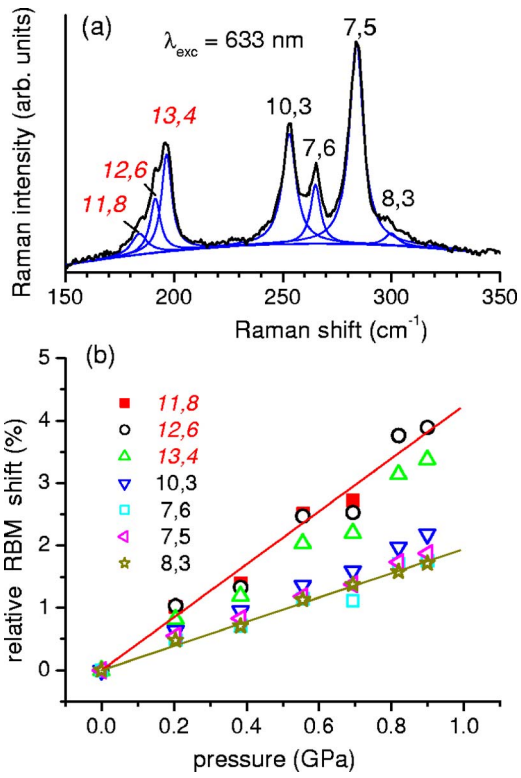

FIG. 3. (Color online) (a) The RBM Raman spectrum of water-1 wt.% sodium cholate dispersion of HiPco nanotubes at ambient pressure as excited at 633 nm (black). Also shown are Lorentzian fits of contributing bands as well as their assignment to (n,m) nanotubes. Italic n,m indices denote metallic nanotubes. (b) RBM frequency shifts under low pressure conditions for the assigned nanotubes (as a percentage of the RBM frequency at ambient pressure). Also shown are linear fits for (12,6) and (8,3) nanotubes.

tubes (filled squares) is less certain because of the limited number of data points and the comparatively large error bars on $d\omega_{RBM}/dP$ values obtained for the three metallic tubes with the largest diameters. Nevertheless, the RBM of metallic tubes appears to be softer (larger values of $d\omega_{RBM}/dP$) compared to semiconducting tubes of a similar diameter (Fig. 4). This unexpected result suggests that mechanical (vibrational) properties of SWNTs depend to some extent on their electronic structure (metallic versus semiconducting).

The observed increase of $d\omega_{RBM}/dP$ with increasing d as well as the magnitude of $d\omega_{RBM}/dP$ are very similar to those found by Venkateswaran *et al.* for a sample of purified *bundled* HiPco nanotubes compressed with methanol-ethanol.[24] These authors argued that tube-tube interactions in SWNT bundles dominate this dependence, since an elastic-continuum model for individual nanotubes predicts the values of $d\omega_{RBM}/dP$ that are much smaller and *inversely* proportional to d.[24] While comparisons of measurements on as-grown and purified (oxidized) SWNTs should be treated with caution, our results suggest that the increase of $d\omega_{RBM}/dP$ with an increasing tube diameter is an intrinsic property of individual nanotubes, *which also shows up in bundles*.

The relatively large values of $d\omega_{RBM}/dP$ observed for both individually dispersed SWNTs (5.2–8.2 cm^{-1}/GPa; this work) and different samples of bundled SWNTs (measured

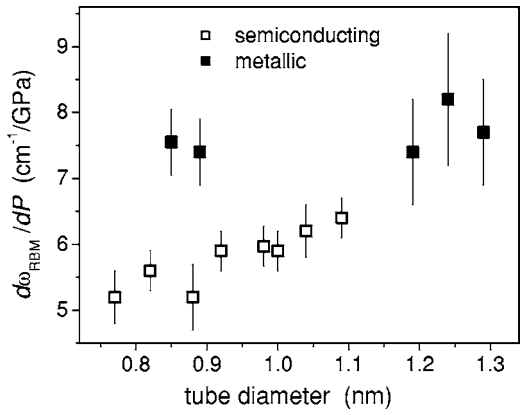

FIG. 4. Pressure derivatives of the RBM frequency of HiPco nanotubes dispersed in water-1 wt.% sodium cholate as determined in the low pressure regime ($\leq$1 GPa) as a function of the tube diameter (see also Table I). Larger error bars relate to relatively weak and poorly resolved RBM bands and corresponding uncertainties of the Lorentzian fits.

between 7 and 11.4 cm^{-1}/GPa)[16,17,19,22–25] draw previous theoretical interpretations of bundle compression into question. Comparable RBM shifts in model SWNT bundles dominated by the intertube van der Waals interactions were calculated by Venkateswaran *et al.*[16] and Kahn and Lu,[38] under the assumption that a bundle is compressed as a whole, i.e., without penetration of a pressure transmitting medium like water or methanol-ethanol into intertube channels. However, as noted by Venkateswaran *et al.*, this assumption is not supported by a number of experimental observations such as the rapid intercalation of SWNT bundles.[16] Furthermore, a decrease of $d\omega_{RBM}/dP$ with increasing tube diameter in model SWNT bundles was predicted[38]—in contrast to the dependence found in this work and in Ref. 24.

The observed dependence $d\omega_{RBM}/dP \sim d$ could, in principle, be explained by the anharmonicity of the phonon mode. Specifically, the circumferential stress in compressed nanotubes and, consequently, the effect of anharmonicity on the RBM frequency are expected to be proportional to d. However, the influence of anharmonicity on vibrations in graphite and carbon nanotubes is generally thought to be negligible.[1] Instead, it may be necessary to invoke interactions between nanotubes and the environment (pressure transmitting medium) in order to explain the RBM pressure dependence. Slightly different interactions with the environment may also explain the systematic difference between the RBM pressure derivatives of metallic and semiconducting tubes (see previous).

C. RBM features at low pressure: Shifts in excitation resonance

Resonance Raman spectra of SWNTs can be strongly affected by shifts of optical transitions under pressure. Kazaoui *et al.* have reported a reversible red shift of the first absorption band (corresponding to E_{11}^S transitions in semiconducting tubes) in SWNT films upon pressurization to 4 GPa.[18] Wu *et al.* have measured absorption of HiPco nanotubes in D_2O-SDS dispersions subject to hydrostatic compression in a DAC at pressures up to $\sim$1 GPa and have found (n,m)-dependent red shifts of absorption bands with pressure derivatives of up to -46 and -16 meV/GPa for assigned E_{11}^S and E_{22}^S-energies, respectively.[39]

Recently, we have performed an analogous experiment to Ref. 39 using PL spectroscopy instead of absorption.[40] This allows a more reliable assignment of (E_{11}^S, E_{22}^S) vs (n,m) as well as the differentiation between individual semiconducting nanotubes and residual bundles, since only the former luminesce. Poorly reproducible and large downshifts of up to -80 meV/GPa were observed for both E_{11}^S and E_{22}^S energies when probing SWNTs in SDS dispersion under pressures up to $\sim$1 GPa. In contrast, reproducible and smaller energy shifts were observed for SWNTs in aqueous sodium cholate or SDBS suspension: (n,m)-dependent pressure derivatives of E_{22}^S (relevant for the excitation range in this work) were between +5 and -30 meV/GPa. In general, smaller E_{22}^S shifts were found for the nanotube family classified by $(n-m)\text{mod } 3=2$ and larger ones for nanotubes with $(n-m)\text{mod } 3=1$.[41] Pressure induced shifts of E_{11}^M transition energies for (nonluminescent) metallic nanotubes were not measurable by PL. Neither have these shifts yet been established by alternate methods.

Despite the relatively small shifts in optical transition energies observed for semiconducting (and probably also metallic) nanotubes dispersed with sodium cholate or SDBS, two new RBM bands could be detected under pressure, as indicated by the asterisks in Fig. 2. Specifically, a band at $\sim$275 cm^{-1} occurs above $\sim$2.5 GPa in the $\lambda_{ex}=785$ nm spectrum and a broad feature at $\sim$200 cm^{-1} is observed above $\sim$1 GPa for $\lambda_{ex}=514$ nm. From Fig. 1 and taking into account the possible RBM frequency shifts, the first band (at $\sim$275 cm^{-1}) can tentatively be assigned to (9,4) nanotubes [the required downshift of the E_{22}^S energy of (9,4) nanotubes is consistent with our PL results]. The second feature presumably corresponds to a group of large diameter semiconducting tubes excited via E_{33}^S optical transitions that are now downshifted closer to the 514 nm excitation line. Analogous new (n,m) resonances in the 633 nm spectra are probably too weak and overlapped to be resolvable in Fig. 2.

The peculiar behavior of SDS dispersions is not yet fully understood.[40] The unusually large pressure induced shifts of optical transition energies lead to more strongly affected Raman spectra than for the other surfactants. For SDS dispersions, significant changes to the RBM Raman pattern at 633 nm excitation were already observed for pressures as low as $\sim$1 GPa. A correlation of the RBM bands with those measured at ambient pressure became unreliable above $\sim$1.5 GPa. Therefore, we limited high pressure measurements to nanotube dispersions prepared with sodium cholate and SDBS.

D. Raman *G* bands in the low pressure regime

Figure 5 presents Raman spectra in the *G* mode region for cholate dispersed HiPco nanotubes under pressure. These are the counterparts to the RBM spectra in Fig. 2. The *G* mode is theoretically composed of six Raman-active tangential vibra-

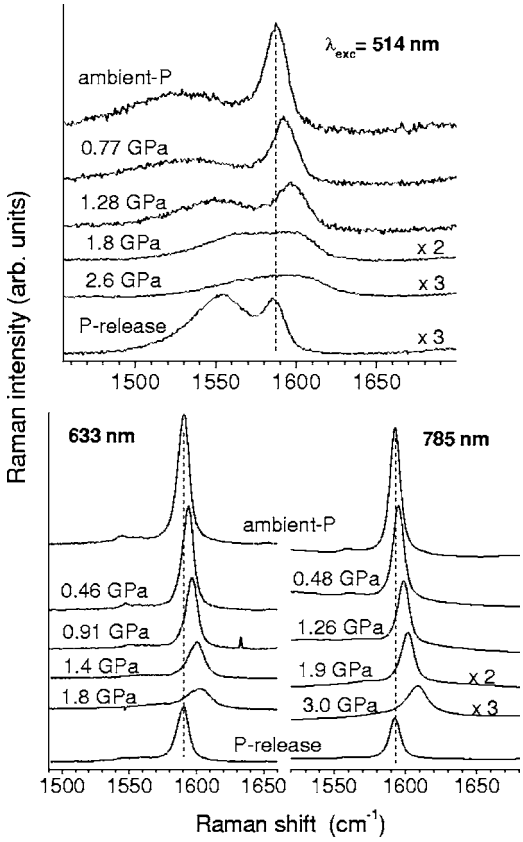

FIG. 5. The pressure dependence of the Raman *G* band of HiPco nanotubes dispersed in water - 1 wt.% sodium cholate and excited at 633, 785, and 514 nm. For each excitation wavelength and sample, the pressure was increased in steps to the largest indicated value and then decreased.

tional modes in SWNTs. Frequencies are only weakly dependent on the nanotube diameter.[42] In practice, the *G* band for individual SWNTs (and even for some SWNT bundles) can be fit by two main components, denoted as $G+$ and G^- for the high- and low-frequency branches, respectively. The *G* band lineshape is characteristically broad for metallic and narrow for semiconducting tubes[42]—as apparent in the Raman spectra of dispersed metallic and semiconducting tubes excited at 514 and 785 nm, respectively (Fig. 5). As both metallic and semiconducting tubes are excited at 633 nm, the corresponding G^- region consists of two weak components and is difficult to analyze. Here, the narrow and intense $G+$ peak appears to be mostly contributed by semiconducting tubes. This *G* band "classsification" scheme remains valid for dispersed tubes compressed up to ~2–3 GPa pressure (Fig. 5). For unclear reasons, the large diameter semiconducting tubes excited via E_{33}^S transitions and assigned in the previous section to a broad feature at ~200 cm^{-1}, which appears in the 514 nm RBM spectra at pressures above ~1 GPa, do not contribute significantly to the *G* band, as excited at 514 nm.

In previous work, the $G+$ and G^- Raman peak components of semiconducting tubes as well as the $G+$ of metallic tubes have typically been fit with Lorentzians, whereas an asymmetric Breit-Wigner-Fano lineshape has usually been applied to the G^- feature of metallic tubes (and bundles).[42] In contrast, the broad but symmetric G^- peaks observed in our measurements for dispersed metallic tubes both at ambient and elevated pressures (Fig. 5, λ_{ex}=514 nm) can be well approximated by a Lorentzian lineshape. This is in accordance with a recent combined Raman and electrical transport study of individual nanotubes.[43]

Upon pressurization up to ~1 GPa, *G* bands manifest reversible linear upshifts in frequency as well as reversible intensity decreases—in parallel to the changes in RBM spectral features already discussed. After further compression to above ~2–3 GPa, a significant irreversible intensity decrease is observed for all *G* bands. This is coupled with a strong modification of the *G* band lineshape for metallic tubes (Fig. 5). Similar to the RBM shifts, pressure derivatives, $d\omega_G/dP$, of the $G+$ frequency (the main component in the *G* mode spectra) were found to depend somewhat on the excitation wavelength [i.e., (n,m) dependence] as well as tube environment (e.g., dispersed versus deposited nanotubes). $d\omega_G/dP$ values for linear $G+$ upshifts in the pressure range <2 GPa were determined as 8.0±0.2, 6.5±0.6, and 8.0±0.5 cm^{-1}/GPa at λ_{ex}=514, 633, and 785 nm, respectively. These are consistent with a wide range of $d\omega_G/dP$ values from 4.5 to 10.1 cm^{-1}/GPa, which have been determined for various samples of as-grown and purified SWNTs *bundles*, as reviewed in Ref. 23.

Pressure derivatives of $G+$ and G^- for metallic tubes under low pressure (<2 GPa) were the same to within experimental error (8.0±0.2 and 8.5±0.8 cm^{-1}/GPa), in accordance with the results for SWNT bundles.[44] The relative shifts of the G^- and $G+$ components under pressure provide useful information for a theoretical description of tangential vibrations of stressed SWNTs.[44] An analysis of the G^- shift for semiconducting nanotubes (λ_{ex}=785 nm) was not attempted because of the poor signal-to-noise ratio for this weak component.

E. High pressure Raman spectra and collapse of nanotubes

Upon compressing aqueous dispersions of SWNTs to beyond ~3 GPa, RBM, and *G* bands, as measured at λ_{ex} =514 and 633 nm become progressively broadened and diminished in intensity. Consequently, the Raman bands of metallic tubes (λ_{ex}=514 nm), which are already relatively weak and broad, even at ambient pressure, become unresolvable at ~4 GPa. In contrast, at 633 nm excitation, the *G* band (mostly contributed by semiconducting nanotubes) can be observed up to ~9 GPa. Note, however, that in this high pressure regime the Raman spectra of aqueous dispersions were poorly reproducible—even for the same sample if measured at different laser spot locations in the DAC. Figure 6(a) illustrates this effect: upon pressurization from ~3–9 GPa, we observe the dramatic broadening of $G+$ (by up to ~150 cm^{-1}) as well as pronounced scatter of the $G+$ maximum between 1600 and 1660 cm^{-1}. We attribute these anomalies to the nonhydrostatic compression of SWNTs due to local shear stresses occurring in aqueous dispersions above the solidification point of water at ~1 GPa at room temperature. Such nonhydrostaticity has been well documented for pressures above ~5 GPa.[33] This effect strongly

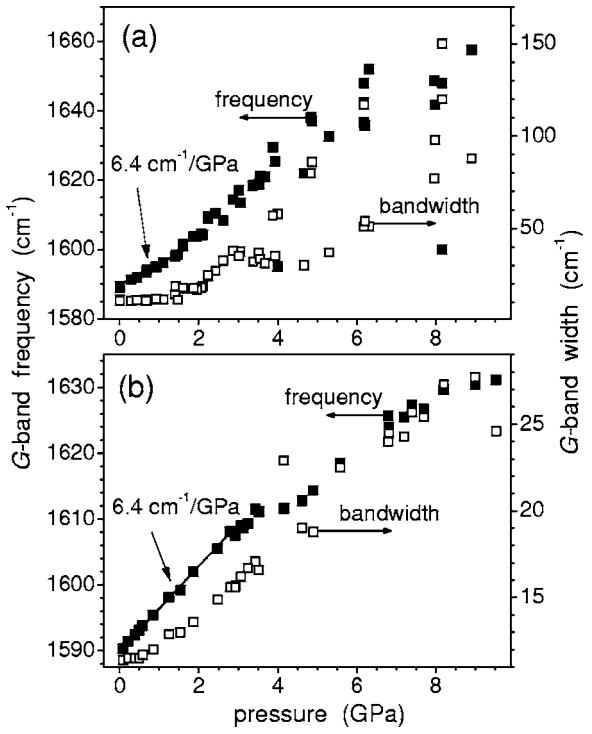

FIG. 6. Pressure dependence of the frequency and bandwidth of the most intense G band component ($G+$) as excited at 633 nm for HiPco nanotubes (a) compressed directly in water-sodium cholate dispersion and (b) deposited onto glass microfibers and compressed using methanol-ethanol. The large datapoint scatter and wide bands above ~3 GPa in (a) arise from nonhydrostatic conditions in solidified aqueous dispersions (see Sec. III E for details).

limits the use of water as a high pressure transmitting medium. Nonhydrostatic effects are likely especially pronounced when pressurizing highly anisotropic objects such as nanotubes—thus rationalizing the onset of anomalous broadening and the scatter of G band features already at ~2–3 GPa [Fig. 6(a)].

The careful deposition of SWNTs from water-surfactant dispersions onto glass microfibers (see Sec. II) was found to preserve the nanotubes in the isolated (debundled) form, as evidenced by Raman and PL spectra. Such water-free samples could be then placed in the DAC and compressed with a standard pressure transmitting medium, which provides good hydrostatic conditions up to ~10 GPa.[33] In this study we used a methanol-ethanol mixture (4:1 v/v). While apparently quite complicated and nonuniform (glass microfibers + surfactant layer + embedded nanotubes + pressure transmitting medium), the observed reproducible shifts of the G band under pressure and its narrow lineshape [Fig. 6(b)] suggest the quasihydrostatic compression of deposited SWNTs can be realized in this configuration. A disadvantage of this sample preparation method is the very small amount of nanotubes (estimated as, at most, several hundred nanotubes in resonance) that can actually be probed in the DAC with the laser microscope. Consequently, the experiments described below were limited to 633 nm excitation because of inherently stronger Raman signals accessible at this wavelength.

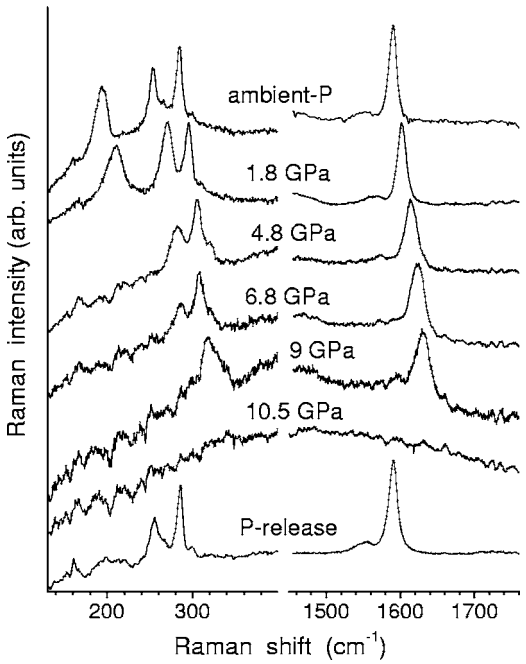

FIG. 7. Pressure dependence of the RBM and G bands for HiPco nanotubes deposited from 1 wt.% sodium cholate dispersions onto glass microfibers and compressed with methanol-ethanol. The excitation wavelength is 633 nm. Each spectrum has been scaled to maximum intensity and is shifted vertically for clarity.

The pressurization induced shift of the G band frequency of HiPco nanotubes deposited onto glass microfibers manifests a characteristic plateau at about ~4 GPa and a decreased pressure derivative above [Fig. 6(b)]. Qualitatively similar behavior has been observed for various samples of bundled SWNTs at different plateau pressures. Amer *et al.* have tentatively ascribed these observations to "adsorption"-like molecular ordering of the pressure transmitting medium around nanotubes.[25] Whether this hypothesis is true or not, we agree with these authors that the plateau or a change in the pressure derivative of the G band cannot reliably be interpreted as a sign of the uniform structural deformation throughout the SWNT sample.

Instead, we regard the relatively abrupt disappearance of *both* G and RBM bands at pressures beyond 10.5 GPa (Fig. 7) as an indication for the onset of dramatic cross-section deformation for a specific subset of nanotubes contained within the sample. To estimate which (n,m) tubes can contribute, we took into account pressure-dependent Raman lineshapes and frequency shifts as well as downshifts in resonance energies (Secs. III C and III G). At high pressures, the G and RBM modes seen in Fig. 7 appear to still be mainly contributed by semiconducting (7,5), (8,3), and probably (8,4) tubes having $d \sim 0.8–0.9$ nm. A critical radial deformation pressure of $P_C \sim 10$ GPa for nanotubes with these diameters corresponds well to theoretical predictions (see the Introduction).

Theory predicts a dependence $P_C \sim 1/d^3$ for individual nanotubes.[10,12,14] Normalizing to our experimental result for $d \sim 0.8–0.9$ nm, we predict $P_C \sim 3.5$ GPa for the group of metallic tubes having $d \sim 1.2–1.3$ nm. These contribute to

the lowest-frequency RBM band as excited at 633 nm [cf. Fig. 7 and Fig. 3(a)]. Indeed, both this RBM feature and the corresponding G^- contribution disappears at ~4 GPa (Fig. 7)—albeit not as abruptly as the bands of semiconducting tubes at ~10 GPa. Further support for the collapse of these tubes is provided by the dramatic changes to the RBM band after pressure release as compared to the spectrum after release of ~2 GPa (Fig. 2). We attribute the irreversible effects to (local) structural damage and/or chemical modification of SWNTs, which could be particularly efficient for collapsed tubes. On the other hand, the irreversible changes to the Raman bands of semiconducting tubes are not as significant after the release of 10.5 GPa (Fig. 6). Possibly, resonance Raman spectroscopy is less sensitive to the additional structural and/or chemical defects generated in the semiconducting tube fraction. We will return to this issue in Sec. III G, which discusses pressure-induced structural deterioration in semiconducting tubes as evidenced by strong irreversible changes to their PL spectra.

Theory also predicts unusual hysteresis effects for radially deformed nanotubes with $d > 1$ nm, which progress with an increasing tube diameter.[14] A Raman study of these possible effects in the vicinity of P_C, also appying other laser excitation wavelengths in order to probe different groups of semiconducting nanotubes, is planned for the future.

F. Raman *D* band intensity

The relative intensity of the defect-induced Raman *D* band at ~1320 cm^{-1} has been widely used as a coarse estimate of the quality of SWNTs.[1,42] Figure 8 shows Raman spectra in the the *D* and *G* band range for nanotubes deposited onto glass microfibers and measured at ambient pressure before and after compression up to 8 GPa. For all laser excitation wavelengths, a significant enhancement of the *D* band relative to the *G* band is observed following compression—providing additional evidence for the structural deterioration of SWNTs under high pressure. Again, this effect is much more pronounced for the metallic (λ_{exc} = 514 nm) than for the semiconducting tubes (λ_{exc} = 785 nm) probed. The spectra excited at 633 nm show an intermediate level of irreversible changes after compression, consistent with contributions from both metallic and semiconducting tubes to the *G* and *D* bands. Note that the spectral shift of the *D* band results from a strong dependence of this vibrational mode on tube diameter and Raman excitation energy.[42] Beyond these excitation wavelength-dependent effects there is a small but significant additional ~3–5 cm^{-1} shift of the *D* band after pressure release, with metallic and semiconducting tubes having opposite signs (Fig. 8). Note also dramatic changes in the lineshape of the *G* band attributed to metallic nanotubes. While the trends are the same, these changes do not quantitatively reproduce those in the Raman spectra of dispersed metallic nanotubes compressed up to ~3 GPa (Fig. 5). This can be related to the different sample forms studied and pressures applied.

The results presented in Fig. 8 provide further evidence that the structural damage of nanotubes starts to occur at compression levels below those inferred for dramatic cross-section distortion (collapse). Indeed, metallic tubes excited at 514 nm ($d \sim 0.85–0.89$ nm) are not expected to deform under pressure of 8 GPa (see Sec. III E). However, they show the most pronounced irreversible effects in the Raman spectra.

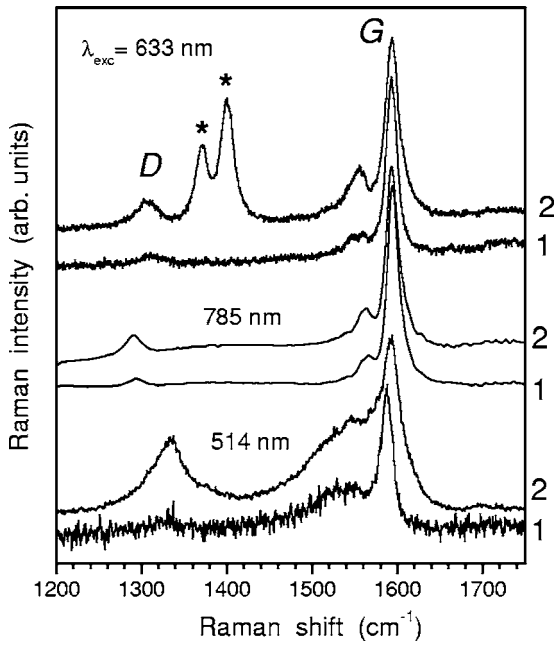

FIG. 8. *D* and *G* bands at different laser excitation wavelengths for HiPco nanotubes deposited from a cholate dispersion onto glass microfibers and measured at ambient pressure. (1) initial sample and (2) the same sample recovered from the diamond anvil cell after compression with methanol-ethanol up to 8 GPa for ~10 min. Each spectrum has been scaled to the *G* band intensity maximum and is vertically shifted for clarity. The asterisks indicate luminescence bands of a ruby microcrystal used for pressure calibration.

It would clearly be interesting to probe for a similar irreversible enhancement of the *D* band for SWNTs compressed in aqueous dispersions. However, we were only able to measure substrate-deposited nanotubes, because these samples (in contrast to fluid dispersions) could be readily recovered from the DAC. A direct measurement of the *D* band of SWNTs within the DAC (under applied pressure) is hindered by the strong Raman line of diamond.

G. Photoluminescence under high pressure

In contrast to metallic nanotubes, the RBM and *G* bands contributed by semiconducting nanotubes recover their shape almost completely, albeit with a ~10- and ~5-fold loss of intensity, respectively, after application of pressure up to ~10 GPa (see the spectra in Figs. 7, 8, excited at 633 and 785 nm). By itself, this observation might lead one to conclude that individual semiconducting SWNTs are fairly resistant to such extreme compression. However, changes to the photoluminescence of semiconducting nanotubes clearly indicate that irreversible structural deterioration already occurs at lower pressures. Here we briefly discuss these effects of pressurization on PL spectra. A detailed PL study of SWNTs under pressure will be published elsewhere.[40]

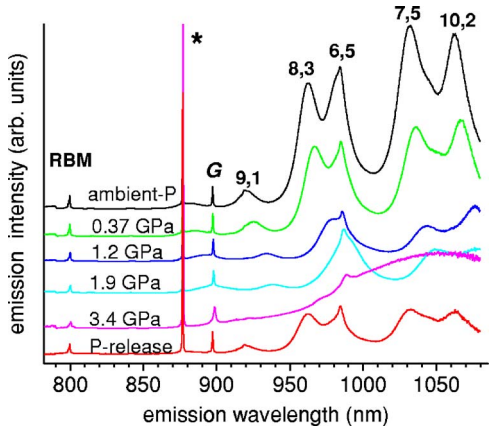

FIG. 9. (Color online) Raman and photoluminescence (PL) emission spectra of nanotubes dispersed in D_2O - 1 wt.% sodium cholate (intensity versus wavelength of emitted/scattered light). Shown are spectra obtained for the same sample at ambient pressure, upon increasing compression and after pressure release. The laser excitation wavelength was 785 nm. The spectra are each scaled to the *G* band intensity maximum and are vertically shifted for clarity. Five PL bands are assigned to the labeled (n,m) semiconducting tubes. The asterisk refers to the Raman line of the diamond anvils.

Figure 9 shows the pressure dependence of Raman and PL bands of dispersed HiPco nanotubes as excited at 785 nm and measured simultaneously over a wide spectral range of up to ~1080 nm. Note that the Raman and PL features in these measurements are contributed by different semiconducting (n,m) nanotubes. Figure 9 illustrates a strong intensity decrease and a dramatic broadening of the PL bands upon increasing pressure up to 3.4 GPa—followed by significant irreversible changes in the PL after pressure release. These changes appear to be stronger for the larger diameter (7,5) and (10,2) tubes (15-fold decrease in PL intensity) as compared to the smaller diameter (9,1) and (8,3) tubes (11- and 9-fold decrease in PL intensity, respectively).

The effects of compression are particularly evident in the PL maps (PL intensity versus excitation and emission wavelengths) measured for different samples of the same SWNT dispersion at ambient pressure, under 4 GPa, and after application and release of 4 and 6.5 GPa pressure, respectively (Fig. 10). These maps were measured in the excitation range of 708–850 nm and now include the PL peaks of (12,1), (11,3), (10,5), and (9,7) nanotubes ($d \sim 1.0$–1.1 nm), which are also the major contributors to the Raman spectra excited at 785 nm. Irreversible peak broadening and the loss of intensity after compression at 4 GPa are more pronounced for these tubes than for (10,2), (9,4), and (8,6) tubes with *d*

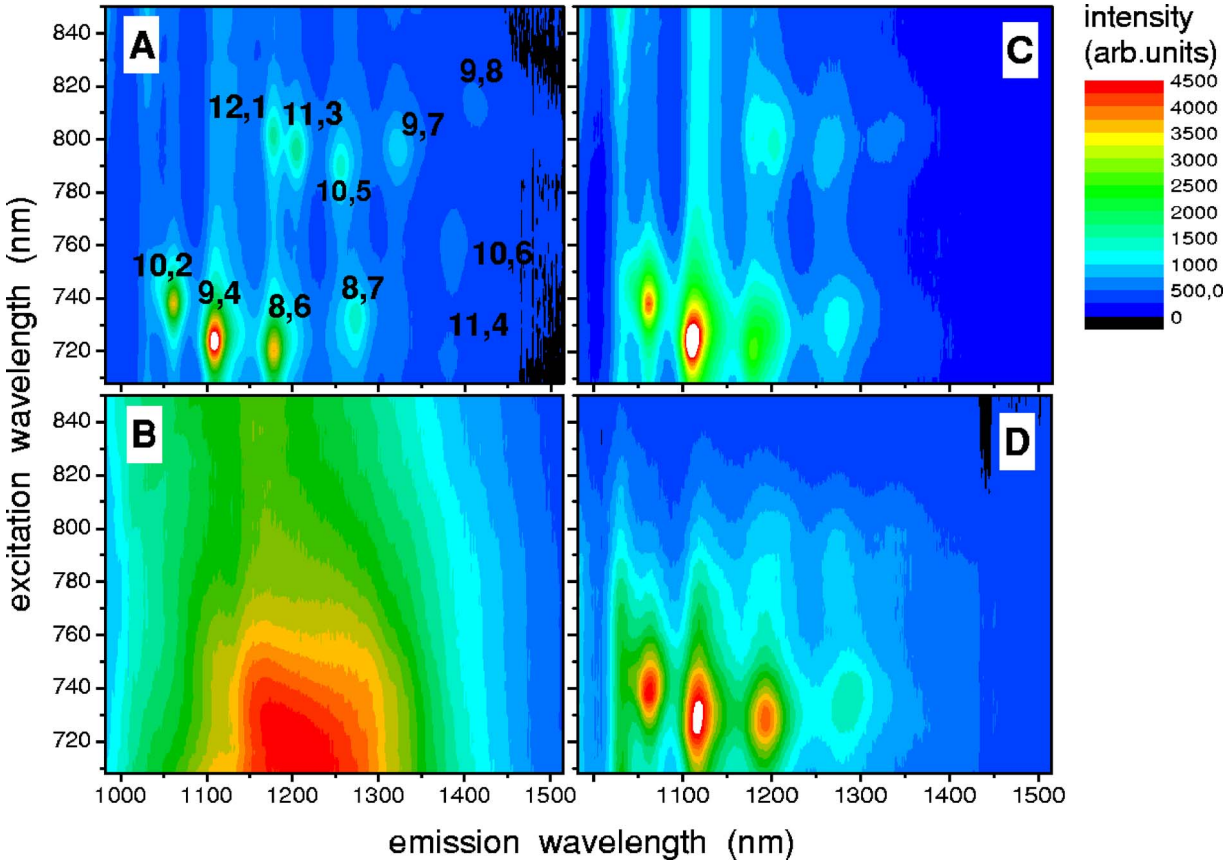

FIG. 10. (Color online) Photoluminescence contour maps (intensity versus excitation and emission wavelengths) for HiPco nanotubes dispersed in D_2O-1 wt.% sodium cholate. The PL emission and excitation maxima correspond to E_{11}^S and E_{22}^S energies, respectively. (A) PL map at ambient pressure with (n,m) indices of emitting semiconducting tubes; (B) under 4 GPa; (C) after 4 GPa pressure release; (D) after compression of a fresh sample up to 6.5 GPa and pressure release. The PL intensity color schemes are linear, but different scaling factors were used for each of the four maps (maximum intensities scale as 25: 1: 6: 2 for A, B, C, and D, respectively).

$\sim 0.87-0.95$ nm [Fig. 10(c)]. From the Raman results discussed in Sec. III E, we do not expect radial deformation to be significant at 4 GPa for the (n,m) nanotubes labeled in Fig. 10(a). For the large diameter tubes ($d \sim 1.0$–1.15 nm), including also (9,8) and (11,4) tubes [Fig. 10(a)], such deformation should occur in the $\sim 6-8$ GPa range. Therefore, stronger structural damage facilitated by radial deformation may explain the disappearance (strong broadening) of the PL peaks of these nanotubes after the application of 6.5 GPa pressure [Fig. 10(d)].

Finally, we note the significant broadening of PL peaks under high pressure. In fact, PL peaks merge into a single feature under 4 GPa compression [Fig. 10(b)]. At this pressure, the estimated broadening of the corresponding E_{22}^S (relevant to the Raman spectra) and E_{22}^S transitions is up to ~ 200 and ~ 100 meV, respectively. This makes an accurate determination of energy shifts impossible. However, a comparison of the PL maps in Figs. 10(a) and 10(b) suggests that shifts in E_{22}^S peak maxima (<100 meV at 4 GPa) are not very large for the group of nanotubes that mainly contribute to PL emission [(10,2), (9,4), and (8,6) nanotubes that belong to the $(n\text{-}m)\text{mod}\,3=2$ family]. As in the broadening of Raman bands (Fig. 6(a)), we attribute a considerable part of the PL broadening in Fig. 10(b) to nonhydrostatic conditions in the solidified aqueous dispersions. Indeed, more structured PL features ($\Delta E_{22}^S \sim 100-150$ meV at ~ 4 GPa) were observed in preliminary measurements of nanotubes deposited on glass microfibers and compressed with methanol-ethanol. Note that the broadening of interband optical transitions found in PL explains, at least to a significant part, theobserved decrease of Raman signals under increasing pressure.

IV. SUMMARY

We have demonstrated that it is possible to study high pressure effects on individually dispersed (debundled) SWNTs by using a DAC and a sensitive Raman apparatus. The problem of nonhydrostatic conditions encountered in solidified aqueous dispersions above $\sim 2-3$ GPa was solved by the deposition of dispersed nanotubes onto inert glass microfibers and by applying a methanol-ethanol mixture as a pressure transmitting medium. Raman and PL spectra indicate that the so deposited nanotubes remain in the isolated (debundled) form. Similar to the results of Venkateswaran *et al.* for SWNT bundles and in contrast with the predictions of a simple elastic-continuum model,[24] we found that the pressure derivative of the RBM frequency increases with an increasing tube diameter. Furthemore, the RBMs of metallic nanotubes appear to be somewhat softer than those of semiconducting nanotubes of a similar diameter.

Our Raman and PL results show that (n,m) resonances can be strongly influenced by shifts and broadening of optical transtions of SWNTs under pressure. This effect, together with the band broadening and loss of Raman scattering intensity, hinders the (n,m) assignment of the RBM spectra above $\sim 2-3$ GPa. On the other hand, the characteristic lineshape of the *G* band indicates that under high pressures it is still possible to differentiate between major contributions from metallic ($\lambda_{ex}=514$ nm) and semiconducting ($\lambda_{exc}=633,785$ nm) nanotubes. The Raman bands assigned to two groups of substrate-deposited nanotubes with $d \sim 1.2-1.3$ and $0.8-0.9$ nm vanish at ~ 4 and ~ 10 GPa, respectively. We infer that this corresponds to the onset of radial deformation of these nanotubes, in accordance with theoretical predictions. Raman bands, in particular of metallic nanotubes, do not completely recover after the application of pressure up to several GPa (and pressure release), even for applied pressures below the threshold for radial deformation. We attribute these irreversible changes in the Raman spectra to structural defects generated in nanotubes. The more pronounced changes for metallic nanotubes may be due to their higher chemical reactivity, e.g., toward a pressure medium or surfactant.[45] Alternatively, the difference may just reflect a higher sensitivity of Raman spectra to added defects in metallic as compared to semiconducting nanotubes. The latter also undergo pressure induced structural deterioration as evidenced by the strong irreversible decrease and broadening of PL peaks, in particular for larger diameter nanotubes.

The nature and formation mechanisms of pressure-induced defects in SWNTs are presently unclear. In addition to the chemical reactions already alluded to, their pronounced generation in water-dispersed SWNTs for compressions much below the predicted collapse pressures may be related to the formation of highly bent tube segments (kinks). This can be rationalized in terms of nonhydrostatic stress in solidified aqueous dispersions, especially at "ice" grain boundaries. Another issue that requires further investigation is the effect of the surfactant wrapping on mechanical (vibrational) properties and on the structural deterioration of nanotubes under pressure. The fact that we are observing radial deformation at critical pressures closely comparable to high-level MD calculations argues that the surfactant does not have a strong influence on overall mechanical properties. Additionally, the good agreement implies that we are probing tube ensembles with a dominant fraction of essentially empty tube segments (i.e., not filled—at least in comparison to the outside density of the pressurization medium). More information could be gained by a comparative study of CVD-grown, surfactant-free individual nanotubes pressurized in a nonreactive medium. Individually dispersed/ deposited SWNTs filled with various substances will also be of future interest (e.g., peapods or double-walled carbon nanotubes[46]).

ACKNOWLEDGMENTS

This work was supported by the Deutsche Forschungsgemeinschaft under SFB 551 and by the Bundesministerium für Bildung und Forschung (BMBF). The authors are grateful to B. Renker for the loan of the DAC and to R. E. Smalley for a sample of HiPco nanotubes.

*Electronic address: lebedkin@int.fzk.de

[1] R. Saito, G. Dresselhaus, and M. S. Dresselhaus, *Physical Properties of Carbon Nanotubes* (Imperial College Press, London, 1998).
[2] S. A. Chesnokov, V. A. Nalimova, A. G. Rinzler, R. E. Smalley, and J. E. Fischer, Phys. Rev. Lett. **82**, 343 (1999).
[3] B. I. Yacobson, C. J. Brabec, and J. Bernholc, Phys. Rev. Lett. **76**, 2511 (1996).
[4] S. Okada, A. Oshiyama, and S. Saito, J. Phys. Soc. Jpn. **70**, 2345 (2001).
[5] S. Reich, C. Thomsen, and P. Ordejon, Phys. Rev. B **65**, 153407 (2002).
[6] O. Gülseren, T. Yildirim, S. Ciraci, and Ç. Kiliç, Phys. Rev. B **65**, 155410 (2002).
[7] M. H. F. Sluiter, V. Kumar, and Y. Kawazoe, Phys. Rev. B **65**, 161402 (2002).
[8] S.-P. Chan, W.-L. Yim, X. G. Gong, and Z.-F. Liu, Phys. Rev. B **68**, 075404 (2003).
[9] S. Reich, C. Thomsen, and P. Ordejon, Phys. Status Solidi B **235**, 354 (2003).
[10] R. B. Capaz, C. D. Spataru, P. Tangney, M. L. Cohen, and S. G. Louie, Phys. Status Solidi B **241**, 3352 (2004).
[11] C. Li and T.-W. Chou, Phys. Rev. B **69**, 073401 (2004).
[12] D. Y. Sun, D. J. Shu, M. Ji, Feng Liu, M. Wang, and X. G. Gong, Phys. Rev. B **70**, 165417 (2004).
[13] X. H. Zhang, D. Y. Sun, Z. F. Liu, and X. G. Gong, Phys. Rev. B **70**, 035422 (2004).
[14] P. Tangney, R. B. Capaz, C. D. Spataru, M. L. Cohen, and S. G. Louie, Nano Lett. (to be published).
[15] J. A. Elliott, J. K. W. Sandler, A. H. Windle, R. J. Young, and M. S. P. Shaffer, Phys. Rev. Lett. **92**, 095501 (2004).
[16] U. D. Venkateswaran, A. M. Rao, E. Richter, M. Menon, A. Rinzler, R. E. Smalley, and P. C. Eklund, Phys. Rev. B **59**, 10928 (1999).
[17] M. J. Peters, L. E. McNeil, J. P. Lu, and D. Kahn, Phys. Rev. B **61**, 5939 (2000).
[18] S. Kazaoui, N. Minami, H. Yamawaki, K. Aoki, H. Kataura, and Y. Achiba, Phys. Rev. B **62**, 1643 (2000).
[19] P. V. Teredesai, A. K. Sood, D. V. S. Muthu, R. Sen, A. Govindaraj, and C. N. R. Rao, Chem. Phys. Lett. **319**, 296 (2000).
[20] J. Tang, L.-C. Qin, T. Sasaki, M. Yudasaka, A. Matsushita, and S. Iijima, Phys. Rev. Lett. **85**, 1887 (2000).
[21] S. M. Sharma, S. Karmakar, S. K. Sikka, P. V. Teredesai, A. K. Sood, A. Govindaraj, and C. N. R. Rao, Phys. Rev. B **63**, 205417 (2001).
[22] S. Rols, I. N. Goncharenko, R. Almairac, J. L. Sauvajol, and I. Mirebeau, Phys. Rev. B **64**, 153401 (2001).
[23] U. D. Venkateswaran, E. A. Brandsen, U. Schlecht, A. M. Rao, E. Richter, I. Loa, K. Syassen, and P. C. Eklund, Phys. Status Solidi B **223**, 225 (2001).
[24] U. D. Venkateswaran, D. L. Masica, G. U. Sumanasekera, C. A. Furtado, U. J. Kim, and P. C. Eklund, Phys. Rev. B **68**, 241406 (2003).
[25] M. S. Amer, M. M. El-Ashry, and J. F. Maguire, J. Chem. Phys. **121**, 2752 (2004).
[26] A. Merlen, N. Bendiab, P. Toulemonde, A. Aouizerat, A. San Miguel, J. L. Sauvajol, G. Montagnac, H. Cardon, and P. Petit, Phys. Rev. B **72**, 035409 (2005).
[27] M. Monteverde and M. Núnez-Regueiro, Phys. Rev. Lett. **94**, 235501 (2005).
[28] M. J. O'Connell, S. M. Bachilo, C. B. Huffman, V. C. Moore, M. S. Strano, E. H. Haroz, K. L. Rialon, P. J. Boul, W. H. Noon, C. Kittrell, J. Ma, R. H. Hauge, R. B. Weisman, and R. E. Smalley, Science **297**, 593 (2002).
[29] F. Hennrich, R. Krupke, S. Lebedkin, K. Arnold, R. Fischer, D. E. Resasco, and M. M. Kappes, J. Phys. Chem. B **109**, 10567 (2005).
[30] F. Hennrich, unpublished data.
[31] S. M. Bachilo, M. S. Strano, C. Kittrell, R. H. Hauge, R. E. Smalley, and R. B. Weisman, Science **298**, 2361 (2002).
[32] M. J. O'Connell, S. Sivaram, and S. K. Doorn, Phys. Rev. B **69**, 235415 (2004).
[33] G. J. Piermarini, S. Block, and J. D. Barnett, J. Appl. Phys. **12**, 5377 (1973).
[34] M. S. Strano, S. K. Doorn, E. H. Haroz, C. Kittrell, R. H. Hauge, and R. E. Smalley, Nano Lett. **3**, 1091 (2003).
[35] H. Telg, J. Maultzsch, S. Reich, F. Hennrich, and C. Thomsen, Phys. Rev. Lett. **93**, 177401 (2004).
[36] C. Fantini, A. Jorio, M. Souza, M. S. Strano, M. S. Dresselhaus, and M. A. Pimenta, Phys. Rev. Lett. **93**, 147406 (2004).
[37] V. Barone, J. E. Peralta, M. Wert, J. Heyd, and G. E. Scuseria, Nano Lett. **5**, 1621 (2005).
[38] D. Kahn and J. P. Lu, Phys. Rev. B **60**, 6535 (1999).
[39] J. Wu, W. Walukiewicz, W. Shan, E. Bourret-Courchesne, J. W. Ager, III, K. M. Yu, E. E. Haller, K. Kissell, S. Bachilo, R. B. Weisman, and R. E. Smalley, Phys. Rev. Lett. **93**, 017404 (2004).
[40] S. Lebedkin, K. Arnold, O. Kiowski, F. Hennrich, and M. M. Kappes, to be published. For preliminary results see: S. Lebedkin, K. Arnold, O. Kiowski, F. Hennrich, and M. M. Kappes, in *Electronic Propeties of Novel Nanostructures*, edited by H. Kuzmany *et al.*, AIP Conference Proceedings Vol. 786 (AIP, Melville, NY, 2005), pp. 124–128.
[41] $p=(n-m) \bmod 3$ is defined here as $n-m=3q+p$, where q is an integer and $p=0,1,2$. Statistically, two thirds of the nanotubes ($p=1,2$) are semiconducting and one third ($p=0$) is metallic.
[42] See, e.g., a recent comprehensive review on the Raman spectroscopy of SWNTs and references therein: M. S. Dresselhaus, G. Dresselhaus, R. Saito, and A. Jorio, Phys. Rep. **409**, 47 (2005).
[43] M. Oron-Carl, F. Hennrich, M. M. Kappes, H. v. Löhneysen, and R. Krupke, Nano Lett. **5**, 1761 (2005).
[44] S. Reich, H. Jantoljak, and C. Thomsen, Phys. Rev. B **61**, R13389 (2000).
[45] M. S. Strano, C. A. Dyke, M. L. Usrey, P. W. Barone, M. J. Allen, H. W. Shan, C. Kittrell, R. H. Hauge, J. M. Tour, and R. E. Smalley, Science **301**, 1519 (2003).
[46] T. Hertel, A. Hagen, V. Talalaev, K. Arnold, F. Hennrich, M. Kappes, S. Rosenthal, J. McBride, H. Ulbricht, and E. Flahaut, Nano Lett. **5**, 511 (2005).